Dirac Half-Metal in a Triangular Ferrimagnet

Hiroaki Ishizuka and Yukitoshi Motome

Department of Applied Physics, University of Tokyo, Hongo, 7-3-1, Bunkyo, Tokyo 113-8656, Japan

(Received 24 August 2012; published 5 December 2012)

An idea is proposed for realizing a fully spin-polarized Dirac semimetal in frustrated itinerant magnets. We show that itinerant electrons on a triangular lattice exhibit the Dirac cone dispersion with half-metallic behavior in the presence of a three-sublattice ferrimagnetic order. The Dirac nodes have the same structure as those of graphene. By variational calculation and Monte Carlo simulation, we demonstrate that the ferrimagnetic order with the Dirac node spontaneously emerges in a simple Kondo lattice model with Ising anisotropy. The realization will be beneficial for spintronics as a candidate for a spin-current generator.

DOI: 10.1103/PhysRevLett.109.237207 PACS numbers: 75.25.−j, 71.10.Fd, 72.25.−b, 73.22.Pr

Massless Dirac fermions show a substantially different nature from ordinary electrons. The peculiar nature originates in the characteristic energy dispersion—the nodal structure with linear dispersion often referred to as the Dirac cone. While the Dirac fermions were originally introduced in relativistic quantum theory, the recent discovery of graphene [1,2], a single layer sheet of graphite, has carved out a new direction of their study in condensed matter systems [3,4]. In graphene, two Dirac cones appear in the energy dispersion of π electrons, which are at the K and K' points in the Brillouin zone for the two-dimensional honeycomb lattice. The Fermi level of this two-dimensional conductor comes right at the nodal points, and the low-energy Hamiltonian is well approximated by the Weyl equation [5]. Various remarkable electronic and transport properties of graphene are the consequences of these Dirac cones in the band structure.

The extraordinary nature of Dirac fermions in graphene has also attracted a great deal of interest from its application to electronics [3]. From the viewpoint of such potential applications, it is of great interest to control the characteristic band structure. Furthermore, it is also desired to control the electronic spin degree of freedom for the application to spintronics [6]. However, there is not as much flexibility in graphene, as the Dirac cone is a direct consequence of the honeycomb lattice geometry and the relativistic spin-orbit interaction is very weak.

In this Letter, we propose an alternative solution for manipulating the spin degree of freedom by seeking possible emergence of Dirac fermions from itinerant magnets. We show that itinerant electrons coupled to a well-known ferrimagnet on a triangular lattice give rise to the Dirac nodes in their band structure, similar to those of graphene. The resultant massless Dirac fermions are spin polarized, and they are stable in a wide range of the spin-charge coupling including typical values in solids. We demonstrate that, by an unbiased Monte Carlo (MC) simulation as well as a variational calculation, such a Dirac half-metal with ferrimagnetic order spontaneously emerges in a minimal Kondo lattice type model. The results strongly suggest the possibility of realizing the exotic electronic state in transition-metal and rare-earth compounds, which generally retain much higher controllable degrees of freedom than graphene. Such a new family will not only add a member to the known list of Dirac electrons in solids [7–10], but will also bring a completely new aspect by the spin polarization. In a half-metal, the electric current is perfectly spin polarized as the low-energy excitations only exist for the majority spin [6]. This nature works as a spin-current generator by filtering out the minority-spin electrons. Thus, our proposal opens a new frontier for the application of massless Dirac fermions, especially for spintronics [11].

Let us first discuss a naive, rather trivial approach to achieve a Dirac half-metal. We here consider a single-band ferromagnetic Kondo lattice model (double-exchange model) on a honeycomb or kagome lattice [see Figs. 1(a) and 1(b)]. The model consists of the nearest-neighbor hopping of electrons and the exchange interaction between the electron spin and the localized moment, whose Hamiltonian is given by

$$H = -t \sum_{\langle i,j\rangle,\sigma} (c^{\dagger}_{i\sigma} c_{j\sigma} + \text{H.c.}) - J \sum_{i} \boldsymbol{\sigma}_i \cdot \mathbf{S}_i. \qquad (1)$$

Here, $c_{i\sigma}$ ($c^{\dagger}_{i\sigma}$) is the annihilation (creation) operator of an itinerant electron with spin $\sigma = \uparrow, \downarrow$ at the ith site, $\boldsymbol{\sigma}_i$ and $\mathbf{S}_i$ represent the itinerant and localized spin, respectively, t is the transfer integral, and J is the on-site Kondo coupling. Hereafter, we take $t = 1$ and $J > 0$.

In this model, when J is sufficiently large compared to the bandwidth at $J = 0$, a ferromagnetic order is stabilized by the double-exchange mechanism in a wide range of electron filling $n = \sum_{i\sigma} \langle c^{\dagger}_{i\sigma} c_{i\sigma} \rangle / 2N$, where N is the system size [12,13]. In the ferromagnetic phase, the band is split in two by the large exchange coupling according to the spin component, and each band has exactly the same form as that for the noninteracting case $J = 0$. Hence, in principle, the Dirac half-metal arises for the honeycomb

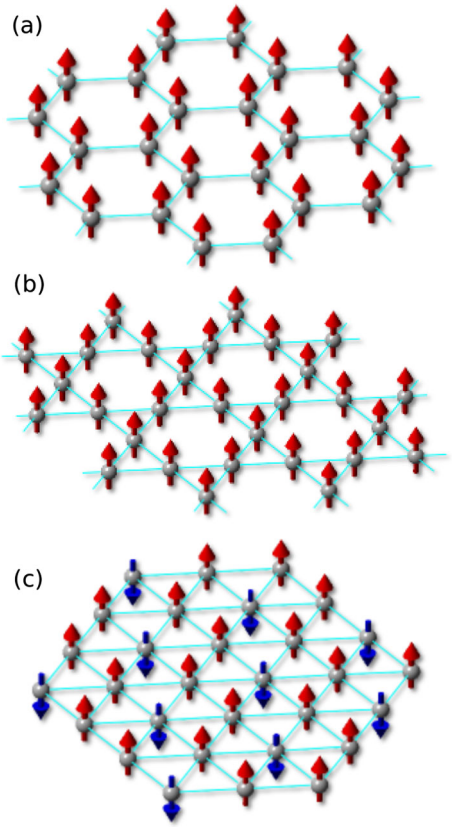

FIG. 1 (color online). Schematic pictures of (a) a honeycomb ferromagnet, (b) kagome ferromagnet, and (c) three-sublattice triangular ferrimagnet. The arrows at each site represent localized spins.

and kagome lattices, as the noninteracting bands on these lattices have the Dirac nodes. However, these situations are very difficult to realize in solids as neither such a strong exchange interaction nor the honeycomb and kagome structures is easily realized in magnetic compounds.

As a more realistic approach, here we propose a simple, but rather nontrivial route to the half-metallic Dirac fermion systems. Let us consider the model in Eq. (1) on a triangular lattice, and the situation in which a three-sublattice collinear ferrimagnetic order with up-up-down spin configuration is realized; see Fig. 1(c). By treating the localized moments as classical spins with $|\mathbf{S}_i| = 1$, the band structure is easily calculated by the exact diagonalization of the Hamiltonian. The lower three bands of the total six bands are shown in Fig. 2; the two bands with upward arrows are of up spins, and the band with downward arrow is of down spin (the other upper three bands have similar form with opposite spins).

The band structure has a notable feature at the energy $\varepsilon = -J$; the two up-spin bands touch each other at the K and K' points in the Brillouin zone to form a Dirac-type point node with linear dispersion, and the down-spin band has the band top at the same points with an ordinary parabolic dispersion. See also the enlarged figure in Fig. 2(b) and the energy dispersion along the symmetric lines in Fig. 2(c).

In this situation, when the electron filling is at $n = 1/3$, the two lower bands are fully occupied while the remaining bands (including the upper three) are unoccupied; the Fermi level is located at the nodes where the three bands meet. As the down-spin band has an energy gap, the half-metallic Dirac electrons are obtained by electron doping to the unoccupied up-spin band. Although hole doping hides the Dirac nature as the down-spin parabolic band is doped at the same time, the situation is avoided by introducing an additional antiferromagnetic exchange coupling between the neighboring sites, $J'\sum_{\langle i,j\rangle}\boldsymbol{\sigma}_i \cdot \mathbf{S}_j$ [14]. A finite $J' > 0$ shifts the down-spin band to the lower energy and isolates the half-metallic Dirac nodes energetically, as demonstrated in Figs. 2(d) and 2(e). Hence, the simple ferrimagnetic order on the triangular lattice realizes the peculiar Dirac half-metallic state near 1/3 filling.

The Dirac nodes have essentially the same structures as those in graphene. Under the ferrimagnetic order, the Hamiltonian is written as

$$\mathcal{H} = \sum_{\mathbf{k}} \begin{pmatrix} -J\sigma_A^z & \tau_{\mathbf{k}} & \tau_{\mathbf{k}}^* \\ \tau_{\mathbf{k}}^* & -J\sigma_B^z & \tau_{\mathbf{k}} \\ \tau_{\mathbf{k}} & \tau_{\mathbf{k}}^* & (J+6J')\sigma_C^z \end{pmatrix}. \quad (2)$$

Here, the upper two rows correspond to the sites with the up localized moment (A, B sublattices) and the bottom row is for the down one (C sublattice) in the three-site unit cell. In Eq. (2), σ^z is the z component of the Pauli matrix for itinerant electrons, $\mathbf{k}$ is the wave vector, and $\tau_{\mathbf{k}}$ is the Fourier transform of the hopping term given by $\tau_{\mathbf{k}} = -t\{e^{ik_x} + e^{i[-k_x/2+(\sqrt{3}/2)k_y]} + e^{i[-k_x/2-(\sqrt{3}/2)k_y]}\}$. By using $\mathbf{k}\cdot\mathbf{p}$ perturbation around the K and K' points in the Brillouin zone [5] and by expanding the result up to the first order in terms of $t\kappa_x/J$ and $t\kappa_y/J$ ($\boldsymbol{\kappa}$ is the relative wave vector measured from the K and K' points), we end up with the low-energy Hamiltonian which is factorized into two parts. One is a 2×2 Hamiltonian for the up-spin honeycomb subnetwork of the A and B sublattices, and the other is a localized state at the down-spin sites in the C sublattice. The former is given by

$$\mathcal{H}_{\mathbf{k}\pm}^{\text{Dirac}} = \begin{pmatrix} -J & \frac{3}{2}it(\kappa_x \pm i\kappa_y) \\ -\frac{3}{2}it(\kappa_x \mp i\kappa_y) & -J \end{pmatrix}, \quad (3)$$

where the sign $\pm$ corresponds to the K and K' points. This has an equivalent form to that of graphene.

It is worth noting that the Dirac nodes are formed immediately by switching on J. However, when J is small, the low-energy physics at $n = 1/3$ is not characterized solely by the massless Dirac fermions because there is a band overlap at the energy of the Dirac nodes. The band overlap comes from the second lower band for up spin, which has an energy minimum at $\mathbf{k} = (2\pi/3, 0)$ and its threefold symmetric points for small J; the minimum energy is given by

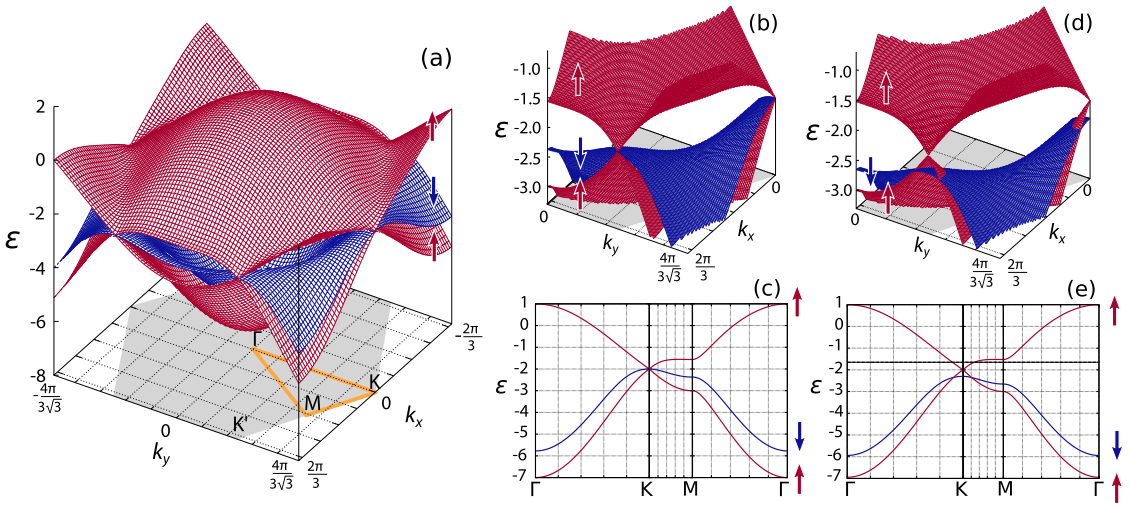

FIG. 2 (color online). Band structures of the model in Eq. (1) under the three-sublattice ferrimagnetic order at $J = 2$. (a) The overall band structure of the three lower-energy bands at $J' = 0$, (b) the enlarged view near the Fermi level $\varepsilon = -J$ at $n = 1/3$ in the first quadrant, and (c) the cut along the symmetric lines. (d), (e) Results at $J' = 0.05$. The arrows indicate the spins for each band. In (a), the gray hexagon on the basal plane shows the first Brillouin zone for the magnetic supercell. The dashed line in (e) indicates the Fermi level in the MC simulation at $T = 0.06$ and $N = 18^2$ shown in Fig. 4.

$\varepsilon_{(2\pi/3,0)} = t/2 + 3J' - \sqrt{(J + 3J' - t/2)^2 + 2t^2}$. In order for the Dirac nodes to be isolated at the Fermi level, this energy should be higher than that at the K and K' points, $\varepsilon_K = -J$. Hence, the Dirac nodes are energetically isolated and play a decisive role when the condition $(J + 3J')/t > 1$ is satisfied. This condition is important because the necessary J and J' are much smaller than the noninteracting bandwidth $9t$, and it is indeed satisfied in a wide range of materials.

Thus far, we assumed the presence of three-sublattice ferrimagnetic order. In the following, we show that such order is indeed stable in the Kondo lattice-type model as in Eq. (1). Here, we simplify the model by assuming the localized moments are the Ising spins taking the values $S_i = \pm 1$.

First, we investigate the ground state phase diagram near $n = 1/3$ by a variational calculation. We compare the ground state energy of the two-sublattice stripe phase and three-sublattice ferrimagnetic phase that appeared in our previous study [15], in addition to the ferromagnetic phase. The results at $J = 2$ are shown in Fig. 3 for $J' = 0$ and 0.05. At $J' = 0$, the ground state in the plotted range is dominated by the ferrimagnetic phase as well as the stripe phase. The different phases are separated by phase separation. As shown in Fig. 3(b), the introduction of small J' largely stabilizes the ferrimagnetic phase near $n = 1/3$ as well as the stripe phase. This is because the itinerant electron spins are polarized parallel to the localized spins in the ground state, leading to an energy gain (loss) by the antiferromagnetic J' for the two states (the ferromagnetic state).

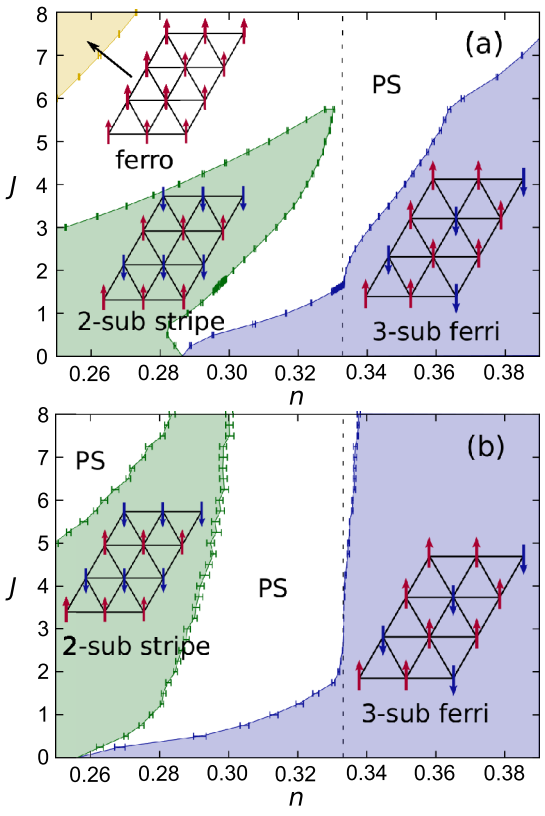

FIG. 3 (color online). Ground state phase diagram obtained by variational calculation at (a) $J' = 0$ and (b) $J' = 0.05$. The schematic picture of magnetic structure in each phase is shown. The white region indicates the electronic phase separation (PS) and the dotted vertical lines indicate $n = 1/3$.

We next examine the stability of the ferrimagnetic order at finite temperatures by an unbiased MC simulation. For the simulation, a standard algorithm for fermion systems coupled to classical fields is used [16]. In this method, the trace over the fermions in the partition function is calculated by the exact diagonalization, while the trace over classical spin configurations is computed by a classical MC method using the METROPOLIS dynamics. The phase transition to ferrimagnetic phase is detected by using two parameters [17]. One is the pseudomoment defined by

$$\tilde{\mathbf{S}}_m = \begin{pmatrix} \frac{2}{\sqrt{6}} & -\frac{1}{\sqrt{6}} & -\frac{1}{\sqrt{6}} \\ 0 & \frac{1}{\sqrt{2}} & -\frac{1}{\sqrt{2}} \\ \frac{1}{\sqrt{3}} & \frac{1}{\sqrt{3}} & \frac{1}{\sqrt{3}} \end{pmatrix} \begin{pmatrix} S_i \\ S_j \\ S_k \end{pmatrix}, \tag{4}$$

where m is the index for the three-site unit cells, and (i, j, k) denote the three sites in the mth unit cell belonging to the sublattices (A, B, C), respectively. We measure the summation $\mathbf{M} = (3/N)\sum_m \tilde{\mathbf{S}}_m$ and the susceptibility. The other is the azimuth parameter ψ defined by $\psi = (\tilde{M}_{xy})^3 \cos 6\phi_M$, where ϕ_M is the azimuth angle of $\mathbf{M}$ in the xy plane and $\tilde{M}_{xy} = 3M_{xy}^2/8$ $(M_{xy}^2 = M_x^2 + M_y^2)$.

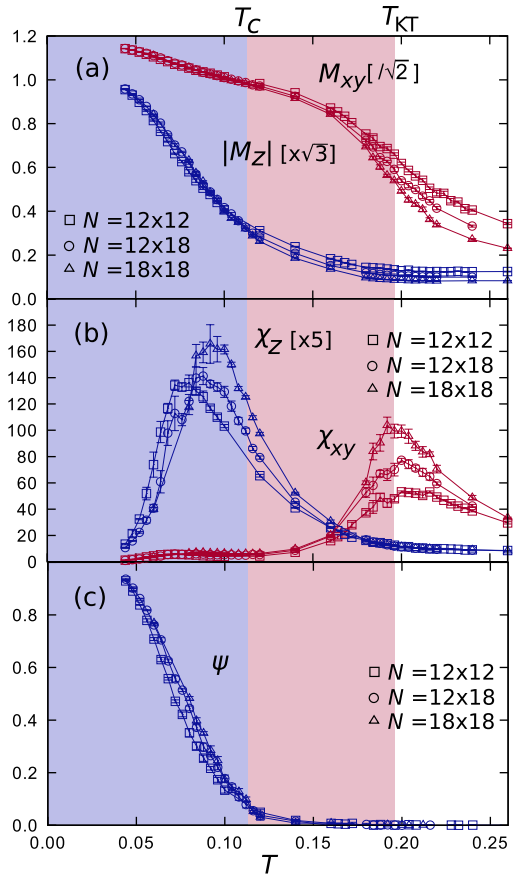

FIG. 4 (color online). MC results for (a) the pseudomoments M_{xy} and $|M_z|$, (b) corresponding susceptibilities χ_{xy} and χ_z, and (c) azimuth parameter ψ. The data are calculated at $n = 0.34$.

The ferrimagnetic ordering is signaled by $M_{xy} \to 2\sqrt{2/3}$, $|M_z| \to 1/\sqrt{3}$, and $\psi \to 1$ at low temperature $T \to 0$, respectively, [15,18,19].

Figure 4 shows the MC results at $J = 2$ and $J' = 0.05$ in the slightly electron doped region to $n = 1/3$ [see also Fig. 2(e)]. The results indicate two successive phase transitions at $T_{KT} = 0.192(15)$ and at $T_c = 0.108(9)$. The transition temperatures are estimated by extrapolating the peak of susceptibilities χ_{xy} and χ_z as $N \to \infty$. The transition at T_{KT} is considered a Kosterlitz-Thouless type with the growth of quasilong-range order [15]. On the other hand, the phase transition at T_c is a three-sublattice ferrimagnetic ordering. The MC result and the above analysis for the ground state consistently indicate that the three-sublattice ferrimagnetic order is stabilized in the vicinity of $n = 1/3$ in the wide range of parameters for J and J', spontaneously giving rise to the Dirac half-metal.

As such ferrimagnetic order was indeed observed in several insulating magnets [20,21], our results in the minimal model will stimulate the hunt for a Dirac half-metal in transition-metal and rare-earth compounds. The present results will be qualitatively robust even when extending the model to more realistic situations. For instance, the ferrimagnetDic state remains stable when including the transverse components of localized spins, at least, in the presence of strong Ising anisotropy. Multiband effects may be avoided under a particular crystal field; for instance, the d-electron a_{1g} orbital isolated by a strong trigonal field is a good candidate for the realization. Interlayer coupling, however, may open a gap at the Dirac nodes. Nevertheless, a straightforward stacking of layers or sufficiently isolated layers in a controlled thin film will be promising to preserve the massless nature.

The authors thank Y. Matsushita, A. Shitade, and Y. Yamaji for helpful comments. H. I. is supported by Grant-in-Aid for JSPS Fellows. This research was supported by KAKENHI (Grants No. 19052008, No. 21340090, No. 22540372, and No. 24340076), Global COE Program "the Physical Sciences Frontier," the Strategic Programs for Innovative Research (SPIRE), MEXT, and the Computational Materials Science Initiative (CMSI), Japan.

[1] K. S. Novoselov, A. K. Geim, S. V. Morozov, D. Jiang, Y. Zhang, S. V. Dubonos, I. V. Grigorieva, and A. A. Firsov, Science **306**, 666 (2004).
[2] K. S. Novoselov, A. K. Geim, S. V. Morozov, D. Jiang, I. V. Katsunelson, I. V. Grigorieva, S. V. Dubonos, and A. A. Firsov, Nature (London) **438**, 197 (2005).
[3] A. K. Geim and K. S. Novoselov, Nat. Mater. **6**, 183 (2007).
[4] For a recent review, see A. H. C. Neto, N. M. R. Peres, K. S. Novoselov, and A. K. Geim, Rev. Mod. Phys. **81**, 109 (2009).

[5] G. W. Semenoff, Phys. Rev. Lett. **53**, 2449 (1984).
[6] S. A. Wolf, D. D. Awschalom, R. A. Buhrman, J. M. Daughton, S. von Molnar, M. L. Roukes, A. Y. Chtchelakanova, and D. M. Treger, Science **294**, 1488 (2001).
[7] M. H. Cohen and E. I. Blount, Philos. Mag. **5**, 115 (1960).
[8] T. Konoike, K. Uchida, and T. Osada, J. Phys. Soc. Jpn. **81**, 043601 (2012).
[9] M. Z. Hasan and C. L. Kane, Rev. Mod. Phys. **82**, 3045 (2010).
[10] S. Ishibashi, K. Terakura, and H. Hosono, J. Phys. Soc. Jpn. **77**, 053709 (2008).
[11] D. Pesin and A. H. MacDonald, Nat. Mater. **11**, 409 (2012).
[12] C. Zener, Phys. Rev. **82**, 403 (1951).
[13] P. W. Anderson and H. Hasegawa, Phys. Rev. **100**, 675 (1955).
[14] An off-site Kondo coupling may exist generally in the Kondo lattice systems, although the magnitude is much smaller than the on-site one and the sign depends on the orbital nature of itinerant and localized electrons. The antiferromagnetic superexchange coupling between neighboring localized spins, given by $J_{\mathrm{AFM}}\sum_{\langle i,j\rangle}\mathbf{S}_i \cdot \mathbf{S}_j$, may also exist, but it neither modifies the band structure nor harms the stability of the ferrimagnetic state.
[15] H. Ishizuka and Y. Motome, Phys. Rev. Lett. **108**, 257205 (2012).
[16] S. Yunoki, J. Hu, A. L. Malvezzi, A. Moreo, N. Furukawa, and E. Dagotto, Phys. Rev. Lett. **80**, 845 (1998).
[17] In principle, the ferrimagnetic ordering can be detected by the spin structure factor. In the finite-size MC calculations for the current model, however, it is useful to employ the pseudomoment and its azimuth parameter for distinguishing it from a three-sublattice partial disorder and Kosterlitz-Thouless–type quasilong-range order. See also Refs. [15,18,19].
[18] H. Takayama, K. Matsumoto, H. Kawahara, and K. Wada, J. Phys. Soc. Jpn. **52**, 2888 (1983).
[19] S. Fujiki, K. Shutoh, S. Inawashiro, Y. Abe, and S. Katsura, J. Phys. Soc. Jpn. **55**, 3326 (1986).
[20] M. Tanaka, H. Iwasaki, K. Siratori, and I. Shindo, J. Phys. Soc. Jpn. **58**, 1433 (1989).
[21] J. Iida, M. Tanaka, Y. Nakagawa, S. Funahash, N. Kimizuka, and S. Takekawa, J. Phys. Soc. Jpn. **62**, 1723 (1993).